JGR Oceans

RESEARCH ARTICLE
10.1029/2019JC015889

Key Points:
- NEMO-OASIS-WRF coupled regional climate model is evaluated and introduced as a new tool for analyzing Tasman Sea climate projections
- NEMO-OASIS-WRF projections suggest that local atmospheric changes drive 73% of the projected 12 Sv increase in EAC extension transport
- The importance of regional changes in wind stress curl driving the enhanced EAC extension is consistent with linear theory

Supporting Information:
- Supporting Information S1

Correspondence to:
C. Y. S. Bull
christopher.bull@northumbria.ac.uk

Citation:
Bull, C. Y. S., Kiss, A. E., Gupta, A. S., Jourdain, N. C., Argüeso, D., Di Luca, A., & Sérazin, G. (2020). Regional versus remote atmosphere-ocean drivers of the rapid projected intensification of the East Australian Current. *Journal of Geophysical Research: Oceans*, *125*, e2019JC015889. https://doi.org/10.1029/2019JC015889

Received 19 NOV 2019
Accepted 17 JUN 2020
Accepted article online 21 JUN 2020

Regional Versus Remote Atmosphere-Ocean Drivers of the Rapid Projected Intensification of the East Australian Current

Christopher Y. S. Bull[1,2,7], Andrew E. Kiss[2,3], Alex Sen Gupta[4,2], Nicolas C. Jourdain[5], Daniel Argüeso[6], Alejandro Di Luca[4,2], and Guillaume Sérazin[4,2]

[1]British Antarctic Survey, Cambridge, UK, [2]ARC Centre of Excellence for Climate Extremes, University of New South Wales, Sydney, Australia, [3]Research School of Earth Sciences, The Australian National University, Canberra, Australia, [4]Climate Change Research Centre, University of New South Wales, Sydney, Australia, [5]University Grenoble Alpes/CNRS/IRD/G-INP, IGE, Grenoble, France, [6]Physics Department, University of the Balearic Islands, Palma, Spain, [7]Now at Department of Geography and Environmental Sciences, Northumbria University, Newcastle upon Tyne, UK

Abstract Like many western boundary currents, the East Australian Current (EAC) extension is projected to get stronger and warmer in the future. The CMIP5 multimodel mean (MMM) projection suggests up to 5°C of warming under an RCP85 scenario by 2100. Previous studies employed Sverdrup balance to associate a trend in basin wide zonally integrated wind stress curl (resulting from the multidecadal poleward intensification in the westerly winds over the Southern Ocean) with enhanced transport in the EAC extension. Possible regional drivers are yet to be considered. Here we introduce the NEMO-OASIS-WRF coupled regional climate model as a framework to improve our understanding of CMIP5 projections. We analyze a hierarchy of simulations in which the regional atmosphere and ocean circulations are allowed to freely evolve subject to boundary conditions that represent present-day and CMIP5 RCP8.5 climate change anomalies. Evaluation of the historical simulation shows an EAC extension that is stronger than similar ocean-only models and observations. This bias is not explained by a linear response to differences in wind stress. The climate change simulations show that regional atmospheric CMIP5 MMM anomalies drive 73% of the projected 12 Sv increase in EAC extension transport whereas the remote ocean boundary conditions and regional radiative forcing (greenhouse gases within the domain) play a smaller role. The importance of regional changes in wind stress curl in driving the enhanced EAC extension is consistent with linear theory where the NEMO-OASIS-WRF response is closer to linear transport estimates compared to the CMIP5 MMM.

Plain Language Summary In recent decades, enhanced warming, severe marine heatwaves, and increased transport by the East Australian Current have led to the invasion of nonnative species and the destruction of kelp forests east of Tasmania. The East Australian Current extension is projected to get stronger and warmer in the future. We seek to better understand coupled climate model projections for the Tasman Sea. This is difficult because there is large model diversity and considerable uncertainty as to how and where future changes will occur. In addition, little is known about the possible importance of regional versus large-scale changes in surface time-mean winds in driving future circulation changes. Here we use a single limited-domain ocean-atmosphere coupled model that takes the average model projections as its inputs and finds that changes in the regional wind stress are most important for the enhanced projected East Australian Current extension. We also find that these projected changes are consistent with simple linear theory and the simulated regional changes in wind stress.

1. Introduction

Globally, the poleward shift of western boundary currents (WBCs) or the intensification of their extensions has led to regional surface warming rates two to three times faster than the global average (Wu et al., 2012; Yang et al., 2016). The Tasman Sea is such a global hotspot (Ridgway, 2007; Ridgway et al., 2008; Wu et al., 2012) where both eddy-permitting ocean-only (Matear et al., 2015; Oliver & Holbrook, 2014) and coarser-resolution ocean-atmosphere coupled climate models (Sen Gupta et al., 2016; Wang et al., 2014; Yang et al., 2016) suggest a stronger East Australian Current (EAC) extension in the future. While direct

in situ observational evidence for WBC intensification over recent decades is limited (Elipot & Beal, 2018; Fernandez et al., 2018), there are many model or reanalysis-based studies (e.g., Biastoch et al., 2009; Cai et al., 2005; Durgadoo et al., 2013; Oliver & Holbrook, 2014; Roemmich et al., 2016; Wu et al., 2012; Yang et al., 2016) that link changes in WBC extensions in the Southern Hemisphere with the multidecadal poleward intensification in the westerly winds over the Southern Ocean (Bracegirdle et al., 2013; Swart & Fyfe, 2012).

The EAC forms the poleward flowing branch of the South Pacific Subtropical Gyre. It transports 22.1 Sv southward at 27°S (Sloyan et al., 2016) with a mean EAC surface core speed of 1.35 m s^{-1} at 30°S (Archer et al., 2017). The EAC exhibits variability over a range of time scales, including a peak at 65–100 days (Archer et al., 2017; Bowen et al., 2005; Mata et al., 2006) corresponding to the shedding of large anticyclonic eddies in the region where the EAC partially separates from the coast. Upon partial separation, a diminished EAC flows eastward forming the Tasman Front (or the "eastern extension of the EAC"; Oke, Pilo, et al., 2019) while the shed eddies migrate south-west toward Tasmania (Everett et al., 2012). In the time-mean, the eddies result in a rectified southward mean flow termed the EAC extension (EACx). Some EACx eddies propagate around Tasmania into the Indian Ocean forming the Tasman Leakage (Baird & Ridgway, 2012; Pilo et al., 2015; Speich et al., 2002). On seasonal time scales the EAC is strongest in summer and weakest in winter (36.3 vs. 27.4 Sv southward transport at 28°S; Ridgway & Godfrey, 1997) with an annual cycle of ~0.55 m s^{-1} about a mean of 1.35 m s^{-1} (velocity in a jet-coordinate frame at 30–31°S; Archer et al., 2017). For a recent review of the Tasman Sea circulation, see Oke, Roughan, et al. (2019).

Observations suggest that the EACx has strengthened and extended ~350 km further southward over the past 60 years (Ridgway, 2007). Based on data between 1944 and 2002, a combination of large-scale warming and enhanced southward advection of warm water has led to a temperature increase in the Tasman Sea of 0.028°C $year^{-1}$ (Ridgway, 2007). In addition, future projections based on CMIP5 coupled climate models suggest a substantial increase (3–10 Sv intermodel spread) in EACx transport between the 20th century and the last part of the 21st century under a business as usual RCP8.5 scenario (Hu et al., 2015; Sen Gupta et al., 2016; Yang et al., 2016). While the CMIP-class models do not simulate the mesoscale features that are ubiquitous in the EAC system, eddy permitting ocean simulations using the 0.1° OFAM (MOM4), forced by climate model projections of surface momentum, heat and freshwater fluxes suggest similar circulation changes to the coarse resolution CMIP models (Chamberlain et al., 2012; Matear et al., 2013, 2015; Oliver et al., 2013, 2015; Oliver & Holbrook, 2014; Sun et al., 2012). Many Tasman Sea studies (e.g., Cai, 2006; Feng et al., 2016; Hill et al., 2011; Oliver & Holbrook, 2014; Sen Gupta et al., 2016) suggest that the EAC circulation response is approximately consistent with linear dynamical theory (Sverdrup/Godfrey Island Rule, GIR; Godfrey, 1989; Sverdrup, 1947), which relates changes in wind stress to changes in depth integrated ocean circulation, based on a number of simplifying assumptions. This approach neglects potential influences from changes in forcing variability, nonlinear responses in the EAC, and air-sea coupling effects, especially those due to mesoscale eddies. In addition, previous climate change attribution studies using the Sverdrup/GIR have not examined the relative importance of regional versus remote changes in wind stress.

Improving our capacity to attribute changes in the EACx to changes in wind forcing necessitates the use of less idealized models of the climate system and forcing. Recent studies have demonstrated the importance of representing mesoscale atmosphere-ocean thermal (Ma et al., 2016) and mechanical (Renault et al., 2016, 2017) feedbacks to improve the mean state of WBCs, including their position and their associated levels of eddy kinetic energy. In particular, the mesoscale atmosphere-ocean feedbacks yield small-scale anomalies of the wind stress curl that contribute to locally shape the oceanic circulation. It is important that the above effects are represented if we want to correctly attribute changes in ocean circulation to changes in forcing in the next generation of eddy-permitting coupled climate models (e.g., Haarsma et al., 2016).

Our goal here is to demonstrate how an eddy-permitting regional coupled climate model can be used to better understand future projections. Past studies have tried to understand projected Tasman Sea circulation changes in terms of the following:

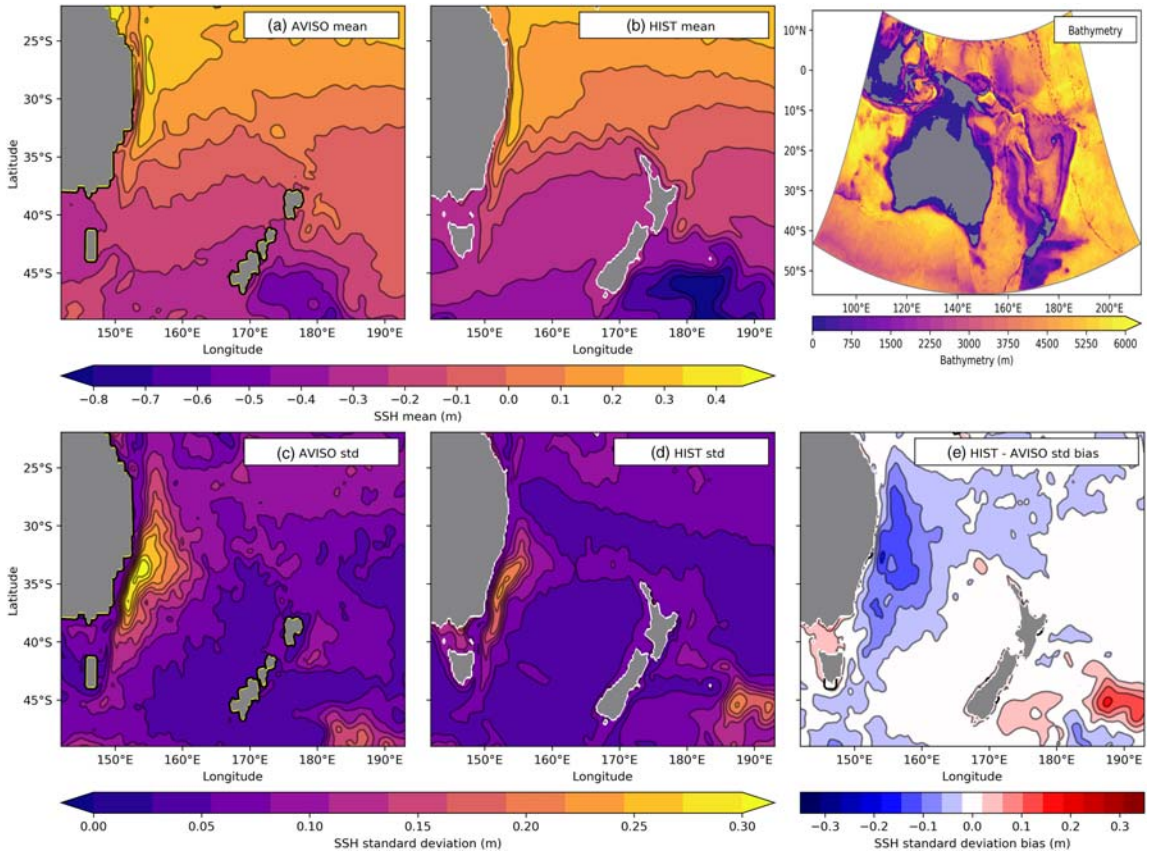

Figure 1. Evaluation of the HIST simulation. Comparison of HIST (b) mean sea surface height and (d) standard deviation with (a, c) AVISO altimetry between 1994 and 2009; both are based on daily values. The area-mean is removed in (a) and (b) to emphasize the difference in mean gradients between HIST and AVISO. Panel (e) shows the standard deviation difference. Bathymetry (top-right) shown to illustrate full NOW domain.

1. Linear theory (Island Rule + Sverdrup). However, this neglects nonlinear dynamics, bathymetry, mesoscale interactions, and changes in buoyancy-driven deep circulation;
2. Coarse resolution coupled climate models. However, these neglect mesoscale activity that is ubiquitous in the EAC system;
3. Forced eddy permitting ocean model simulations. However, these neglect possible air-sea feedback processes (e.g., thermal current feedback).

Here we use the NEMO-OASIS-WRF (NOW) coupled regional climate model extending from the south eastern Indian to the south western Pacific (see section 2.1) with a hierarchy of simulations in which the regional atmosphere and ocean circulations are allowed to freely evolve (domain pictured in top-right Figure 1). The regional simulations are subject to high-frequency boundary forcing, derived from reanalysis with perturbations added based on seasonally varying CMIP5 RCP8.5 climate change anomalies to investigate future changes. This is the first study to use an eddy-permitting (regional) coupled atmosphere-ocean model to analyze projected changes to the EAC and western South Pacific. We examine the following:

1. The fidelity of the historical mean state ocean simulation compared to observations and ocean-only forced simulations;
2. Differences in the circulation change in our eddy-permitting model (forced by CMIP5 at the boundary) and projections from coarse-resolution CMIP5 models;
3. The relative importance of the regional and remote ocean, atmosphere, and radiative forcing in driving the projected changes.

The paper is presented as follows: model description and experiment design are in sections 2.1 and 2.2, respectively. Model evaluation is in section 3.1–3.2. Results contextualizing the NOW simulations in terms

of CMIP5 and understanding the dominant role of the regional atmosphere in the projections are given in sections 3.3 and 3.4 respectively. Discussion and opportunities for further work are given in section 4.

2. Model and Experimental Design

2.1. The Coupled NOW Model, Domain, and Configuration

We use the NOW ocean/atmosphere coupled regional model developed by Samson et al. (2014). The NOW configuration used here comprises NEMOv3.4 (Madec, 2012) for the ocean, WRFv3.5.1 (Skamarock et al., 2008) for the atmosphere, and OASIS3-MCT2 (Valcke, 2013) as a coupler. The NEMO ocean model solves the incompressible, Boussinesq, hydrostatic, primitive equations on a *z*-coordinate C-grid with a filtered free surface and free-slip lateral boundaries. The WRF atmospheric model includes the same parameterizations as in Li et al. (2016), except for convective processes which are parameterized using the Betts-Miller-Janjić scheme (Janjić, 1994). Every hour, the oceanic and atmospheric components exchange physical fields through the OASIS coupler, including sea surface temperature (SST), surface ocean velocity, wind stress, heat fluxes (sensible, latent, longwave, and shortwave radiation), and freshwater fluxes (precipitation minus evaporation). The wind stress formulation is based on relative winds thereby accounting for ocean surface currents (Oerder et al., 2016).

Here NEMO uses 75 vertical levels with partial cells, where there are 24 levels in the first 100 m and 22 levels between 100 and 1,000 m to realistically represent coastlines and continental shelves. The NEMO configuration here is similar to the one used by Bull et al. (2017, 2018) (same domain, model version, present-day ERA-Interim (ERAI) forcing, parameterizations, ocean bathymetry, and model mesh) but differs in that Bull et al. (2017) was ocean-only, forced directly with fluxes, with absolute winds, and Bull et al. (2018) used bulk formulas. An additional difference is that both Bull et al. (2017, 2018) used 5-day mean for the ocean boundary conditions whereas NOW uses daily. BULL-2017 and BULL-2018 will hereafter refer to historical NEMO simulations from Bull et al. (2017, 2018), respectively.

WRF and NEMO share the same horizontal grid mesh (Arakawa C-grid) covering the full CORDEX Australasian domain (https://www.cordex.org/domains/region%20109%2010australasia/), which covers Indonesia, Australia, New Zealand, and the South-Western Pacific (pictured in Figure 1) using a grid cell meridional length of 24.5 km and a width varying with latitude between 19.5 and 24.5 km. As such, the ocean is eddy-permitting but cannot fully resolve mesoscale variability (Hallberg, 2013). The ocean bathymetry is from ETOPO1 (Amante & Eakins, 2009) and is adjusted to either zero or 3.5 m where needed to obtain an exact match between the land/sea masks of WRF and NEMO. The few closed seas, bays, and straits that are too narrow to be properly resolved by NEMO are considered as land in NEMO and have prescribed SST in WRF (interpolated from ERAI).

2.2. Experimental Design

The historical 1989–2009 NOW control experiment (hereafter HIST) was produced by integrating the NOW model using reanalysis-based products at the boundaries. Specifically, 6-hourly varying lateral boundary conditions for atmospheric fields (wind velocity, potential temperature, specific humidity, geopotential height) from the ERAI reanalysis (Dee et al., 2011) and daily varying lateral boundary conditions for oceanic fields (ocean velocity, potential temperature, practical salinity) from the ORCA025-L75-MJM95 global simulation (Barnier et al., 2011) which is itself forced by ERAI. ERAI and ORCA025-L75-MJM95 were used as they have been successfully used for regional modeling studies around Australia (e.g., Bull et al., 2017, 2018; Di Virgilio et al., 2019; Di Luca et al., 2016) and show relatively small biases for the region. For example, Dussin et al. (2012) show the absolute SST bias for ORCA025-L75-MJM95 is less than 0.5°C in the Indo-Pacific region (their Figure 18) for the 2000–2009 period, which is small given that no data assimilation is used.

In order to assess plausible future changes, we create future lateral boundary conditions by adding the CMIP5 ensemble mean future changes to the boundary conditions from ERAI/ORCA. Anomalies corresponding to projected changes are added to all atmospheric and oceanic variables needed to run the NOW model (as above), taking into account the seasonal variations in the projected changes. The resulting experiment (hereafter RCP85) is designed to represent conditions over the period 2080–2100 according to the RCP8.5 scenario. The anomalies are calculated as the difference between 1989–2009 and 2080–2100 monthly climatologies (i.e., a repeating 12-month cycle) based on a CMIP5 multimodel mean (MMM) from 33 models

Table 1
List of NOW and NEMO Experiments

	Forcing					
	Atmospheric boundary (WRF)		Ocean boundary (NEMO)		Greenhouse gasses	
Experiment name	ERAI	+RCP85 Anomaly	ORCA025	+RCP85 Anomaly	Present Day	+RCP85
HIST	✓		✓		✓	
RCP85-ATM	✓	✓	✓		✓	
RCP85-OCE	✓		✓	✓	✓	
RCP85-RAD	✓		✓		✓	✓
RCP85	✓	✓	✓	✓	✓	✓
BULL-2017[a]	✓		✓		✓	
BULL-2018[a]	✓		✓		✓	

Note. Experiments differ from HIST by a perturbed boundary forcing, as indicated by red tick marks (✓).
[a]Ocean-only simulations using almost the same NEMO configuration as NOW from (Bull et al., 2017, 2018).

(supporting information Table S1), the result is then interpolated in time to the highest frequency of the boundary conditions, so the changes vary smoothly within a month. This subset of the CMIP5 ensemble is considerably coarser than the NOW configuration with a mean resolution of 1.2° × 1° (further model details are provided in Table S1 and example circulation of the Tasman Sea is shown in Figure S1 of Sen Gupta et al., 2016, for IPSL-CM5A-MR and NorESM1-ME).

This method to define future boundary forcing was used in previous regional atmosphere simulations (e.g., Knutson et al., 2008; Sato et al., 2007; Walsh, 2015) but to our knowledge, never in coupled ocean-atmosphere regional simulations. This approach is an effective way of downscaling the CMIP5 MMM mean while keeping realistic synoptic and interannual variability. It was shown to perform well through perfect-model evaluation (Yoshikane et al., 2012). In addition, this method provides a baseline climate that does not contain the systematic mean-state and seasonality biases that affect individual CMIP5 models (e.g., Figure S2 and Table S2 in Sen Gupta et al., 2016). Recent work by Krinner and Flanner (2018) supports this methodology by showing that CMIP5 models have stationary biases (the projections keep the signature of their present-day bias) for their large-scale tropospheric atmospheric circulation under strong greenhouse forcing (4xCO2). There are of course some associated caveats: our method precludes any future changes in synoptic and interannual variability (e.g., more frequent extreme ENSO events in a warmer climate; Cai et al., 2018). Also, by using a single set of boundary conditions (i.e., based on the MMM), we are also not able to investigate the projection uncertainty stemming from the, sometimes very large, differences in the CMIP5 model projections (Sen Gupta et al., 2016).

To understand the relative importance of the oceanic and atmospheric parts of the imposed climate change perturbation, we run three additional experiments where the climate change anomaly is applied to each component of the modeling system independently (Table 1), namely:

1. the atmosphere *lateral* boundaries only (RCP85-ATM);
2. the longwave radiation scheme *within the regional domain* only (RCP85-RAD);
3. the ocean *lateral* boundaries only (RCP85-OCE).

Estimated concentrations of the five greenhouse gases (CO2, N2O, CH4, CFC11, and CFC12) based on the RCP85 scenario protocol supply forcing to the Rapid Radiative Transfer Model longwave radiation scheme within the regional domain for the RCP85-RAD and RCP85 simulations whereas present-day (1989–2009) greenhouse gas concentrations are used in HIST, RCP85-ATM, and RCP85-OCE simulations. All NOW and NEMO simulations analyzed in this study are listed in Table 1.

Experiments are started from rest with initial conditions from ORCA025-L75-MJM95. Similar to other regional configurations (e.g., Bull et al., 2017; Li et al., 2016; Samson et al., 2014), experiments are conservatively spun-up for 5 years (in this case January 1989 to December 1993), and all results presented in this study use daily-averaged model output from 16 years of integration after spin-up (January 1994 to December 2009).

3. Results

3.1. NOW Evaluation: How Does HIST Compare to Observations and Other Modeling Studies in the Tasman Sea?

In Figure 1 the HIST control simulation is evaluated with respect to satellite altimetry (AVISO) over 1994–2009 when the available observations and simulation overlap. In the time-mean (Figures 1a–1b), the simulated EACx is clearly visible in the Tasman Sea and has a similar structure and along-shore gradient to the observations, with the exception that the poleward end of the EAC extends further south along the Tasmanian coast. New Zealand's East Auckland Current (labeled in Figure 5a) is also clearly visible in HIST. The Tasman Front is more pronounced in HIST compared to AVISO which is a common feature in other models simulating the Tasman Sea (e.g., Oliver & Holbrook, 2014; Ypma et al., 2016). Comparing Figure 1 to similar NEMO stand-alone simulations (Figure 2 in both BULL-2017 and BULL-2018), HIST has an EACx that reaches further south toward Tasmania suggesting that HIST has a larger EACx bias than BULL-2017 and BULL-2018.

The spatial structure of sea surface height variability in the Tasman Sea in NOW reproduces many of the features found in AVISO (Figures 1c–1e), particularly in open sea regions. Around Tasmania and in the Coral Sea, HIST also shows a small improvement in variability biases as compared to similar ERAI ocean-only forced NEMO configurations (Figure 2 in both BULL-2017 and BULL-2018). The HIST variability magnitude however is underestimated by as much as 50% in some parts of the EAC region. This bias is not uncommon in eddy-permitting models that do not fully resolve mesoscale eddies (e.g., Bull et al., 2018; Ypma et al., 2016).

Depth-integrated time-mean (1994–2009) transports from HIST, BULL-2017, BULL-2018, CMIP5, and observations in the Tasman Sea are shown in Figure 2. Section end points are the same as in BULL-2017 and BULL-2018. It should be noted that the time periods for the observational transport estimates taken from Oliver and Holbrook (2014) do not match the model output. The calculated net transport out of the Tasman Sea bounded by A-F is 0.3 Sv for HIST, smaller than the imbalances of 0.5 ± 2, -0.8, 0.6, and 1.5 Sv in Ridgway and Godfrey (1994), CARS, Ypma et al. (2016), and Oliver and Holbrook (2014), respectively.

The core net EAC transport across FE is 28.8 Sv at 28°S in HIST, which is similar to the transport estimates 27.4 (RG94) and 25.8 Sv (CARS) and marginally stronger than 25.5/24.3 Sv for BULL-2017/BULL-2018, respectively (Figure 2). Both model and observations have similar seasonality with maximum southward transports in Austral summer exceeding 35 Sv and minimum southward transports in winter of less than 22 Sv at 28°S (comparing Figure 12 section GH in Ridgway & Godfrey, 1997, with section FE in Figure S2). Other modeling estimates of EAC transport range between 17.5 and 30 Sv (Kiss et al., 2020; Oliver & Holbrook, 2014; Sen Gupta et al., 2016; Wang et al., 2013; Ypma et al., 2016). The transport for the EACx along AB (Figure 2) is strongly overestimated in HIST (18.5 Sv) compared to RG94/CARS (8.1/9.7 Sv, respectively). Interestingly, NEMO-only simulations which are more tightly constrained by observed winds (ERAI) have smaller biases across section AB with transports of 13.9 and 12.7 Sv for BULL-2017/BULL-2018, respectively, but still overestimate transport. This overestimation is also found at section JK at the southeastern tip of mainland Australia and for the Tasman outflow section IH and is consistent with the EACx extending too far to the south, as seen in the sea surface height field (Figures 1a–1b).

The NOW model projections are forced by seasonal anomalies based on the projected CMIP5 MMM along the atmosphere and ocean NOW boundaries. As such, differences between HIST and NOW forced by CMIP5 MMM anomalies relate exclusively to regional processes occurring within the CORDEX domain. For this reason, we now compare HIST and the CMIP5 MMM historical simulation. HIST and other high resolution Tasman Sea simulations (Oliver & Holbrook, 2014; Ypma et al., 2016) have a weaker Tasman Front and stronger EACx compared to the CMIP5 MMM (Figure 2, transects DG and AB). This is partly due to some of the sampled CMIP5 models having a northward flowing EACx (attributed to a northward bias in the latitude of the maximum midlatitude westerlies) and a complete EAC separation at ~30°S (Sen Gupta et al., 2016). In addition, the coarse resolution of many of the CMIP5 ocean models is known to affect transports in eddy-rich WBC regions (e.g., Loveday et al., 2014).

3.2. NOW Evaluation: Can Linear Theory Be Used to Explain the Strong EACx in HIST?

To determine whether the linear response to differences in surface wind stress between NOW HIST and ocean-only BULL-2017/BULL-2018/ORCA025-L75-MJM95 (ORCA025) can explain the simulated

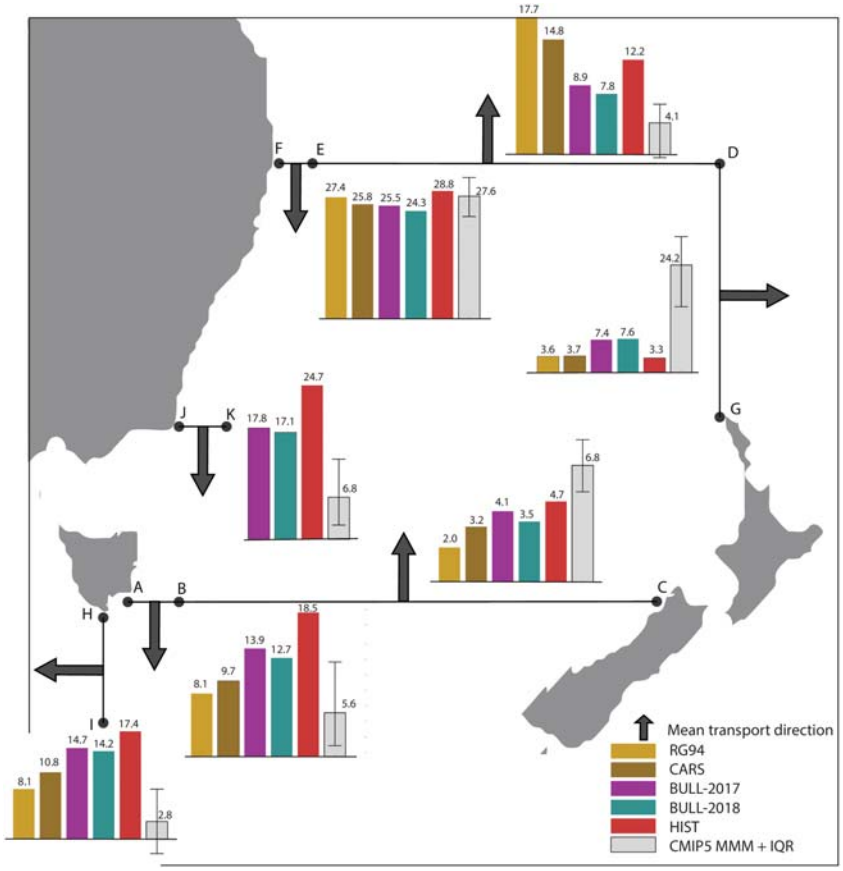

Figure 2. Comparison of HIST (red) mean depth-integrated transport with observations (browns), BULL-2017 (magenta), BULL-2018 (green), and 32 CMIP5 models (gray) where the bar indicates the interquartile range. Units are Sverdrups. HIST transports are depth-integrated to 1945 m. Section end points are similar to Oliver and Holbrook (2014) but sections are aligned with the curvilinear model grid (not strictly zonal/meridional); transport is calculated using grid, normal velocities. The section end points are: A (148.2°E 42.6°S), B (150.8°E 42.6°S), C (172.5°E 40.6°S), D (171.3°E 25.8°S), E (155.6°E 27.6°S), F (153.6°E 27.8°S), G (173.6°E 34.9°S), H (146.9°E 43.4°S), I (146.9°E 45.8°S), J (150.1°E 37.1°S), and K (151.7°E 37.1°S). As the resolution and location of the coast vary across individual CMIP5 model, sections are matched as closely as possible to the NOW sections. The observational estimates are also taken from Oliver and Holbrook (2014), who adapted the eastern edge of the box from Ridgway and Dunn (2003) and Ridgway and Godfrey (1994) (RG94) and the CSIRO Atlas of Regional Seas (CARS) climatology (Ridgway et al., 2002) to enable comparisons to model outputs. All products include Ekman transport aside from CARS.

differences in the EACx transports, we calculate the associated steady-state Sverdrup/GIR (Godfrey, 1989; Godfrey & Dunn, 2010; Sverdrup, 1947; Wajsowicz, 1993) stream function (Ψ_{GIR}; Figure 3 and Table 2). This linear theory estimates the depth-integrated transport purely from the wind stress, assumes a steady state with no friction away from the fast-flowing WBCs, and neglects buoyancy-driven overturning. While this simple theory neglects important nonlinear processes including the inertial overshoot of the EAC, it is an instructive first step for understanding the response of the circulation to wind changes, before considering more complex dynamics. To calculate the HIST Ψ_{GIR}, we follow the regional method used in BULL-2018, namely, outside the NOW regional domain, the ORCA025 wind stress is used (ERAI forcing); inside the NOW model domain, the simulated (WRF) wind stress is used. By construction then, any differences in the GIR-inferred estimate of EAC transport must come from differences in the wind stress curl field inside the NOW domain. GIR values published in BULL-2018 and Oliver and Holbrook (2014) were approximated by using a single line integral around Australia, New Zealand, and the South Pacific (essentially Figure 15 in Szoeke, 1987), whereas all GIR streamfunction values here were calculated using the modified island rule that takes into account the presence of multiple islands (in this case Australia and New Zealand; Godfrey & Dunn, 2010; Wajsowicz, 1993), inferred EAC transport estimates are ~0.8 Sv higher as a result.

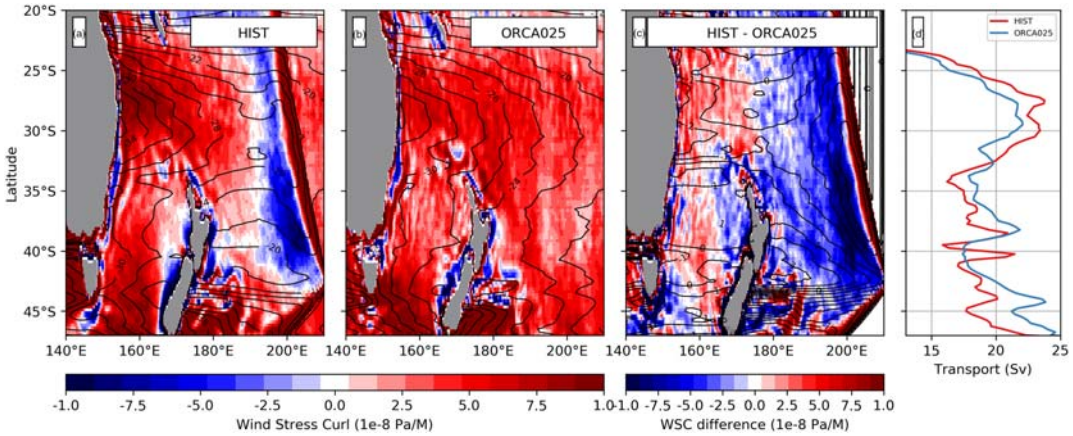

Figure 3. (a–c) Analytical Godfrey Island Rule stream function (Ψ_{GIR}) (solid contours every 1 Sv) and wind stress curl (colors) for (a) HIST, (b) ORCA025, and (c) HIST-ORCA025 difference. (d) Inferred EAC transports.

We now consider two questions:

1. Does Ψ_{GIR} accurately predict EAC transport in HIST and BULL-2017/BULL-2018 compared to transport obtained directly from model velocity?
2. Is there a GIR difference in EACx transport between HIST and ORCA025/BULL-2017/BULL-2018? In other words, are the EACx transport differences explained by the linear response to wind?

On the first question, for the upstream EAC (FE), GIR-inferred HIST transport is too weak compared to the model (23.7 vs. 28.8 Sv in Table 2a). However, the GIR-inferred ocean-only ORCA025 simulation transports at FE are 1.5–2.4 Sv weaker still, suggesting that the stronger model transport in HIST (compared to BULL-2017/BULL-2018) is partly due to a linear response to differences in regional wind stress curl. HIST transports are well-predicted by the GIR for both the EACx (AB) and net Tasman sea transport (ABC), but the BULL-2017/BULL-2018 simulations have much weaker transport than is predicted by the GIR. This mismatch is not surprising as the GIR is known to perform poorly in the EACx region where EACx transport is driven by nonlinear eddy rectification. The GIR-predicted net southward transport across ABC in Table 2a is roughly double the observational estimate of 7.4 Sv (Ridgway & Dunn, 2003). Our results are consistent with Tilburg et al. (2001) and Ridgway and Godfrey (1994) who also obtained large linear transport estimates of 12.1 and 15 Sv, respectively.

On the second question, the EACx overestimate is now evaluated by comparing the HIST and ORCA025 wind stress curl (ORCA025 was also used in BULL-2017 and BULL-2018). Figure 3c shows that there are large differences in the HIST and ORCA025 (ERAI forcing) wind stress curl fields. Compared to

Table 2
(a) NEMO-Modeled and Godfrey Island Rule (GIR)-Inferred Tasman Sea Transports; (b) GIR Streamfunction Values for Australia and New Zealand

(a)

	Model transport			GIR-inferred transport			
	HIST	BULL-2017	BULL-2018	HIST	ORCA025	BULL-2017	BULL-2018
AB	18.5	13.9	12.7	18.8	20.0	20.0	20.4
ABC	13.8	9.8	9.2	14.4	15.0	15.1	15.3
FE	28.8	25.5	24.3	23.7	21.6	21.3	22.2

(b)

	HIST	ORCA025	BULL-2017	BULL-2018
Australia	13.1	12.4	12.8	12.6
New Zealand	27.5	27.4	27.9	27.9

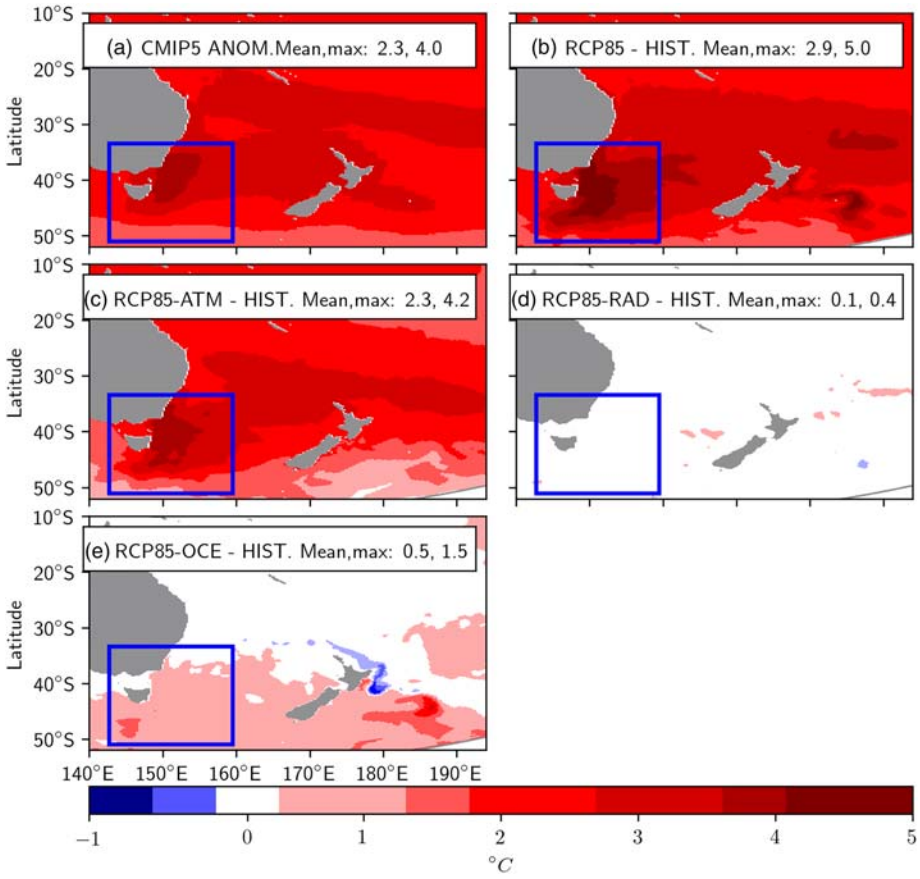

Figure 4. (a) Time-mean sea surface temperature difference between present day and RCP85 in the CMIP5 33 member multimodel mean (see section 2.2) used to force the NOW RCP85 simulation. (b–e) Time-mean sea surface temperature difference between the perturbed climate change forcing and HIST. Mean and maximum values of EACx blue box given in each panel.

ORCA025, HIST has increased wind stress curl north-east and south-east of Australia and weaker curl further east. HIST also has a spurious positive/negative meridional band of curl along the NOW eastern boundary (Figure 3a). The GIR-inferred estimate of EAC transport in HIST in ORCA025 (Figure 3d) integrates these differences, and shows that south of the partial separation at ~34°S, ORCA025 has *increased* GIR transport compared to HIST, with the exception of a narrow peak in transport in HIST at ~40°S. The solid contours showing the Ψ_{GIR} HIST-ORCA025 difference in Figure 3c show that this small peak in transport at ~40°S is due to regional differences in wind stress curl. In addition, the inferred New Zealand island rule transport (Table 2) shows little difference between simulations (with a range of 27.4–27.9 Sv) suggesting that larger differences in transport in the EACx must result from wind stress curl differences in the Tasman Sea on the western side of New Zealand, not from the spurious curl along the NOW eastern boundary in Figure 3a. In summary, the wind stress curl differences and linear theory cannot explain the differences seen in the velocity-based transports from HIST and BULL-2017/BULL-2018 in the EACx. These differences in the HIST simulation will be revisited when interpreting the projections in section 4.

3.3. Future Projected Temperature and Circulation Changes in the Tasman Sea

An intensified warming in the Tasman Sea between 1900 and 2008 has already been observed, with SST warming rates 2–3 times faster than the global mean (Wu et al., 2012). Previous studies (e.g., Figure 6b in Yang et al., 2016) have found enhanced projected warming in the Tasman Sea in the future that has been ascribed to a simulated intensification of the EACx (e.g., Sen Gupta et al., 2016). Consistent with these previous studies, warming in the RCP85 simulation (Figure 4b) and the CMIP5 RCP85 MMM (Figure 4a) relative to the historical period is considerably stronger in the south-western Tasman Sea. However, the temperature

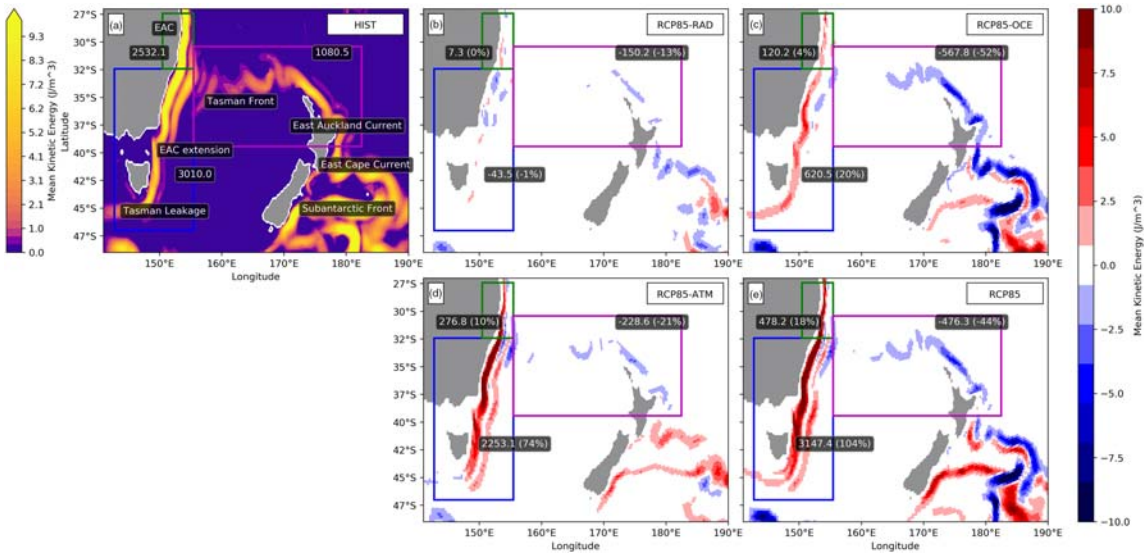

Figure 5. Volume-averaged mean kinetic energy (MKE) for (a) HIST and (b–e) difference from HIST for future climate change scenarios. $\mathrm{MKE}(x, y) = \frac{\rho_0}{2D}\int_{-D}^{0} \left(\overline{u}^2(x, y, z) + \overline{v}^2(x, y, z)\right) dz$, where $\overline{u}$ and $\overline{v}$ are the time-mean horizontal velocity components, $\rho_0 = 1035\ kg\ m^{-3}$, and D is the depth of the seafloor or 1,945 m, whichever is shallower. Highlighted boxes indicate the area used for the total calculated MKE of the following: EAC (green), EAC extension (blue), and Tasman Front (magenta) regions, where (a) total MKE and (b–e) has MKE difference from HIST in J/m^3 (% change).

increase in the EACx reaches 5°C in RCP85 which is 1°C warmer than the CMIP5 MMM, consistent with a stronger intensification of the EACx in NOW compared to CMIP5 MMM (discussed below).

Based on the single boundary forcing experiments, it is clear that the majority of the projected warming signal is driven by changes at the atmospheric boundary (Figures 4c–4e). In the EACx region (blue box), RCP85-ATM projects a 2.3°C mean warming (Figure 4c) compared to 0.5°C from the ocean boundary experiment RCP85-OCE (Figure 4e) and a small 0.1°C from the radiative forcing RCP85-RAD experiment despite RCP85-RAD being associated with increased radiative forcing due to the addition of CO2, CH4, NO2, and CFCs within the domain (Figure 4d). The remote ocean boundary experiment RCP85-OCE shows stronger changes to the east of New Zealand. The total change in RCP85 is very similar to the linear combination of the individual forcing experiments, for example, in the EACx region the 2.9°C RCP warming can be broken down into 2.3°C (RCP85-ATM) + 0.5°C (RCP85-OCN) + 0.1°C (RCP85-RAD). Figure S1 reveals the drivers of these differences in more detail by showing the changes in heat fluxes across the experiments. We can see that the broad-scale warming is primarily associated with increases in net long wave; net short wave and latent heat changes are however important in some regions. Interestingly, of the sensitivity experiments, the change in long wave is strongest in RCP-ATM despite no imposed changes in radiative forcing from anthropogenic greenhouse gases (within the domain). In contrast, in RCP-RAD, the net long wave increase is relatively small. This can be explained by the fact that air entering the domain at the boundaries in RCP-ATM (RCP-RAD) will contain heat and moisture corresponding to the 2080–2100 (historical) period and the large long wave response is most strongly driven by the radiative forcing effect of water vapor. In summary, we see that the projected SST increase in our regional configuration is almost entirely determined by the lateral atmospheric (dominant) and oceanic boundaries with little effect from the regional radiative forcing.

The RCP85 simulations show a doubling in the depth-averaged mean kinetic energy (MKE) in the EACx region (blue box in Figure 5e, an increase of 3,147 J m^{-3}). Similar to the temperature changes (Figure 4), the MKE change in the EACx is a near linear combination of the individual forcing experiments: −43.5 (RCP85-RAD) + 620.5 (RCP85-OCN) + 2253.1 (RCP85-ATM) = 2830.1 J m^{-3}. The changes are spatially similar between RCP85-ATM and RCP85 along the coast of Australia (Figures 5d–5e), suggesting that perturbations applied to the atmospheric boundary are the main driver of change in the Tasman Sea, with the ocean boundary playing a lesser role. All experiments show a weaker Tasman Front (magenta boxes) and modest changes in the upstream EAC (green boxes). Again, to the east of New Zealand the role of the ocean boundary perturbations dominates; this will be analyzed further below.

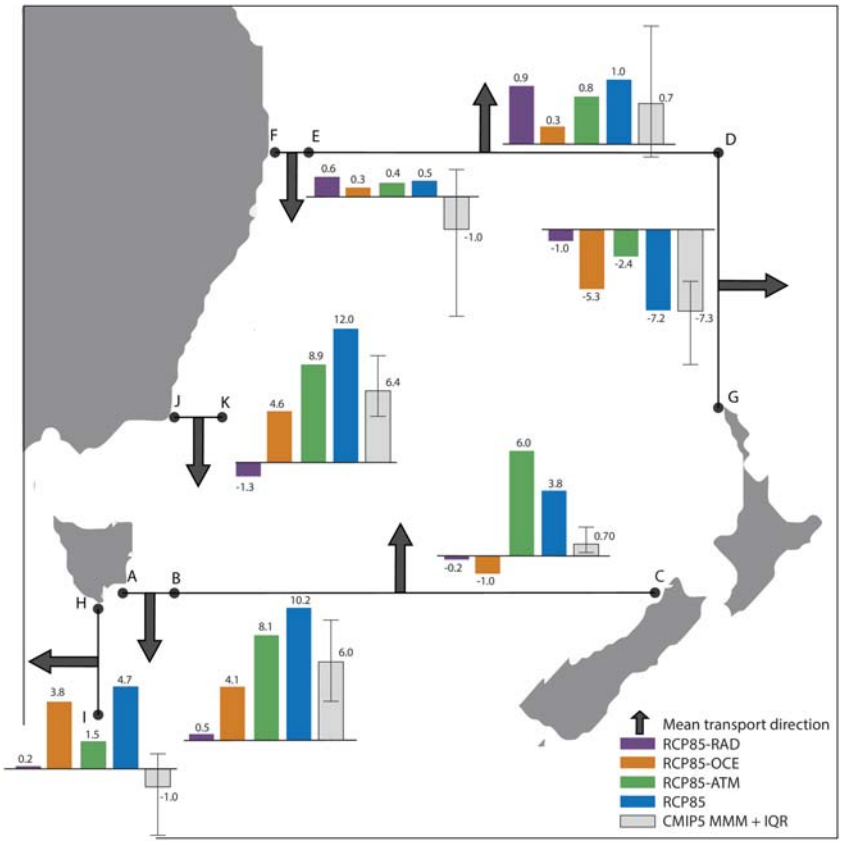

Figure 6. As for Figure 2 but for climate change experiment components and CMIP5 MMM; time-mean transport differences from HIST where arrows indicate net direction of HIST (absolute values in Figure 2).

There is little change in upstream EAC transport in any of the NOW simulations (e.g., <3% or <0.6 Sv at section FE, Figure 6). This is consistent with the CMIP5 models which also indicate only small changes with an equivalent MMM weakening of 1 Sv from a historical mean transport of 27.6 Sv (Figure 2). This is also consistent with the eddy-resolving ocean projections of Oliver and Holbrook (2014) who found little change (a 0.2 Sv, 0.7%, increase along the same section), although this was based on a different (SRES A1B) scenario. As with the CMIP5 and the eddy resolving model, the NOW EAC response is considerably stronger further south (across JK and AB; Figure 6). Across JK, there is an increase of 12 Sv for RCP85. The response and contribution of each experiment is similar across AB and JK. As for SST and MKE, at JK, the total change is almost equal to the sum of the individual boundary forcing experiments: 8.9 (RCP85-ATM) − 1.3

Table 3
Wind Stresses Used to Calculate Ψ_{GIR} (Following the Regional Method Used in BULL-2018) in Figures 7 and 8

	Forcing region	
Experiment name	Wind stress within CORDEX	Wind stress east of CORDEX
ORCA025	ERAI (ORCA025)	ERAI (ORCA025)
HIST	HIST WRF	ERAI (ORCA025)
RCP85-ATM	RCP85-ATM WRF	ERAI (ORCA025)
RCP85-OCE	RCP85-OCE WRF	ERAI (ORAC025) + CMIP5 MMM RCP8.5
RCP85	RCP85 WRF	ERAI (ORAC025) + CMIP5 MMM RCP8.5
CMIP5-HIST	CMIP5 MMM Historical	CMIP5 MMM Historical
CMIP5-RCP85	CMIP5 MMM RCP8.5	CMIP5 MMM RCP8.5
CMIP5-RCP85-OCE	CMIP5 MMM Historical	CMIP5 MMM RCP8.5
CMIP5-RCP85-ATM	CMIP5 MMM RCP8.5	CMIP5 MMM Historical

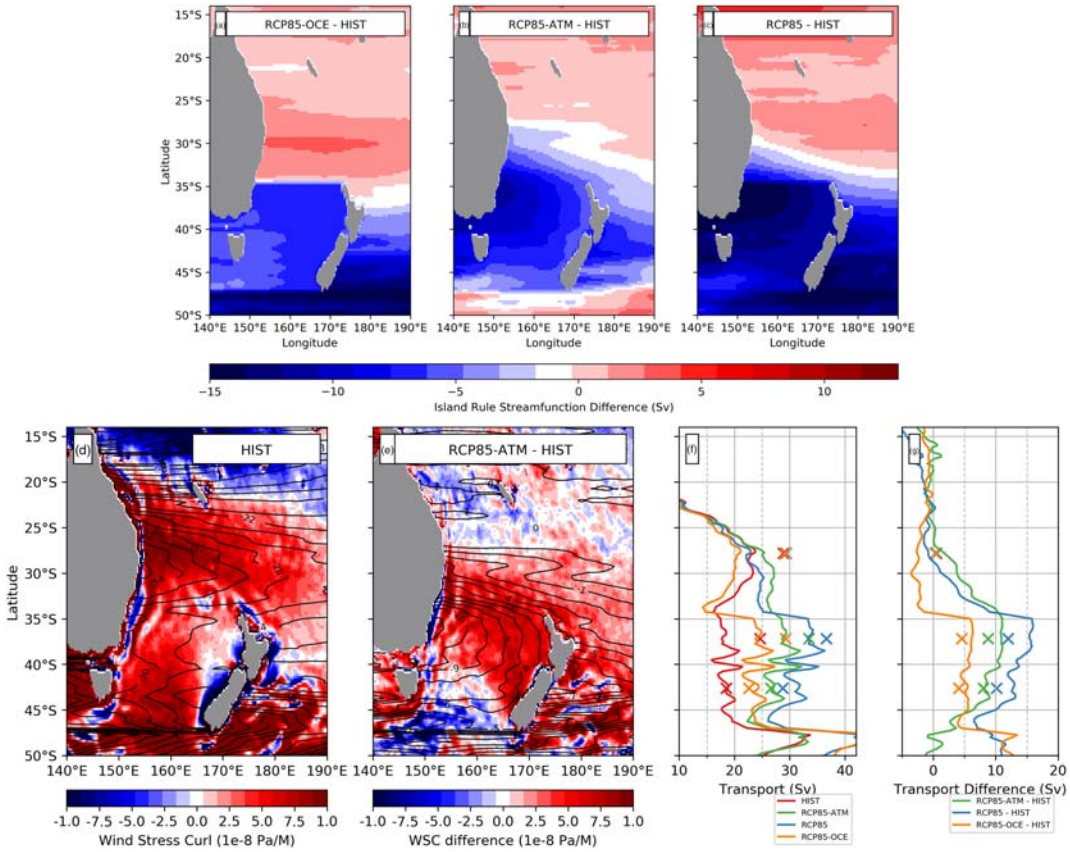

(h)

Experiment	Australia	NZ
HIST	13.1	27.5
RCP85-OCE	13.6	34.3
RCP85-ATM	12.8	32.9
RCP85	13.0	38.2

Figure 7. (a–c) Difference of RCP85-OCE, RCP85-ATM, RCP85 Godfrey Island Rule stream function (Ψ_{GIR}) from HIST. (d) HIST wind stress curl (colors) and Ψ_{GIR} (solid contours). (e) RCP85-ATM–HIST wind stress curl difference (filled) and Ψ_{GIR} difference (solid). (f–g) Inferred EAC transports where subplot f shows differences from HIST and crosses indicate NEMO model transports from Figure 6. (h) Island Rule values for Australia and New Zealand across the experiments.

(RCP85-RAD) + 4.6 (RCP85-OCE) = 12.2 Sv. This equates to the atmospheric boundary forcing being responsible for 73% of the changes in mean transport at JK. Since the RCP85-RAD has relatively little effect on EAC transport, MKE, and SST in the Tasman Sea, it is excluded from further analysis.

Qualitatively both the NOW model and the CMIP5 models suggest little change to the upstream EAC, and a substantial enhancement of the EACx partly at the expense of transport along the Tasman front. Specifically, there is a MMM 6.4 Sv (94%) increase in transport at JK and a 7.3 Sv (30%) decrease in the Tasman Front across DG. However, NOW's RCP85 simulation has a considerably stronger EACx response compared to the median change from the CMIP5 simulations, although some individual CMIP5 models have larger changes that are comparable to the NOW model (Sen Gupta et al., 2016). The NOW EACx response will be examined in section 3.4.

3.4. Understanding NOW and CMIP5 Circulation Changes Using the Sverdrup/GIR

Previous studies (e.g., Oliver & Holbrook, 2014; Sen Gupta et al., 2016) have suggested that changes in EAC transport are approximately consistent with basin-wide changes in the wind stress field. It is curious then

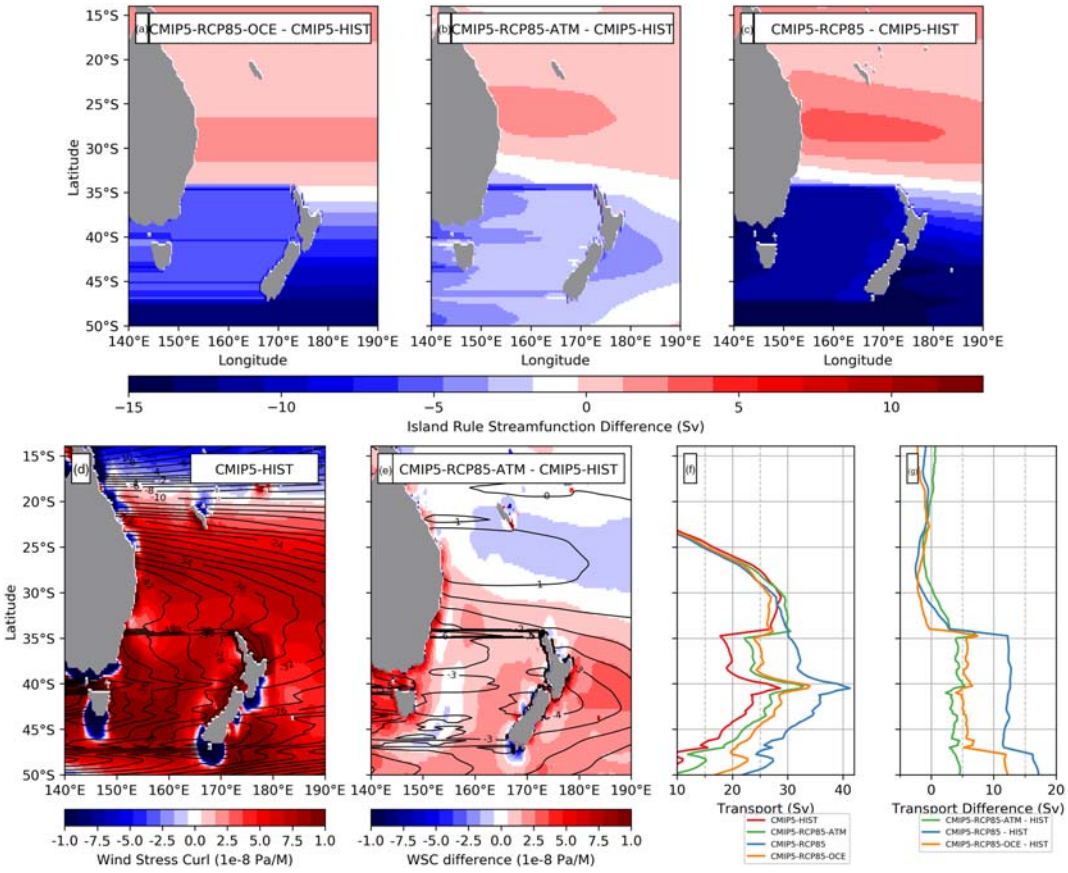

(h)

Experiment	Australia	NZ
CMIP5-HIST	15.6	27.1
CMIP5-RCP85-OCE	15.2	29.3
CMIP5-RCP85-ATM	16.0	33.1
CMIP5-RCP85	15.2	37.5

Figure 8. Like Figure 7 the Ψ_{GIR} but now with the CMIP5 multimodel means using CMIP5 historical simulations as a baseline.

that changes in the ocean boundary conditions have such a small role in the intensification of the EACx in the RCP85 experiment, given that any wind-driven circulation changes to the east of the domain boundary would be communicated to NOW via the ocean boundary conditions and the model domain extends over less than half the width of the Pacific basin. To examine how changes in projected surface wind stress affect the ocean circulation in our CMIP5 based simulation projections, we estimate the steady-state Ψ_{GIR} (based on two-island GIR and Sverdrup calculations) for the NOW experiments. To estimate Ψ_{GIR} we require wind stress fields that are consistent with each simulation's forcing (Table 3). While this method is consistent with the forcing of the regional model, it assumes that the circulation change applied at the boundary is purely a result of linear wind-driven changes, which is reasonable as studies have shown that the circulation is largely determined by Sverdrup dynamics in the gyre interior (e.g., Gray & Riser, 2014). We also neglect the influence of the regional radiative forcing as we have found in section 3.3 that its influence on the EACx and Tasman Sea circulation is small. The Ψ_{GIR} for NOW and CMIP5 model forcings are shown in Figures 7 and 8, respectively.

The RCP85 inferred linear wind-driven projected change in the Ψ_{GIR} is shown in Figure 7c. Consistent with the projected transport changes, enhanced anticyclonic circulation (i.e., a "spin-up" of the mean circulation) is found south of about 30°S, with a weak enhanced cyclonic circulation to the north. The enhanced

circulation in the Tasman Sea can be largely explained by the regional western Pacific wind changes (Figure 7b) and a broad positive wind stress curl anomaly stretching eastward from the southeastern Australian coast toward New Zealand (Figure 7e). Based on the inferred changes representative of the ocean forced simulation (RCP85-OCE; Figure 7a) there is a weaker anticyclonic anomaly south of 35°S that acts to reinforce the stronger EACx change associated with the RCP-ATM simulation, with a cyclonic anomaly north of this. The anomaly in the Tasman Sea in Figure 7a from RCP85-OCE is largely independent of longitude and so is likely due to the change in the New Zealand Island rule streamfuncton value (Figure 7h), which in turn is due to changes in the wind stress east of New Zealand, including east of the NOW domain.

The difference between historical and projected Australian two-island rule transport (i.e., the net equatorward transport in the South Pacific) is small (<0.8 Sv for both the full forcing and separate forcing experiments; Figure 7h). So despite changes in regional transports there is little expected change in the wind-driven component of the Indonesian Throughflow transport (although Sen Gupta et al., 2016, show that changes in deep circulation cause a substantial decrease in Indonesian Throughflow transport in the CMIP5 models, independent of Pacific wind changes). Comparing the inferred wind-driven and NOW EAC (JK at 37°S in Figure 6) transport changes (Figure 7g), we find that linear theory predicts changes that are too strong (15.5 vs. 12.0, 10.9 vs. 8.9, and 5.8 vs. 4.6 Sv for RCP85, RCP85-ATM, RCP85-OCE, respectively). However, the proportion of transport attributable to the different climate change components is in good agreement.

Figure 8 shows the analytically calculated Ψ_{GIR} and associated transports for the CMIP5 MMM. To compare with the NOW experiments, we separate the inferred wind-driven circulation changes into parts associated with projected changes within and to the east of the CORDEX domain (Table 3). Unlike the NOW experiments, we are unable to exclude the influence of regional radiative forcing, however for NOW this was shown to be small compared to the other forcing components. Interestingly, while the projected CMIP5-RCP85-OCE (Figure 8a) response is similar to RCP85-OCE (Figure 7a), the projected CMIP5-RCP85-ATM (Figure 8b) response is considerably weaker than for the inferred NOW changes (Figure 7b). This is associated with a weaker positive wind stress curl anomaly in the south-west Pacific (Figure 8e) compared to the NOW simulation (Figure 7e). In terms of EACx transport, this means that the effect of western Pacific wind stress has about equal importance to eastern Pacific wind stress in the CMIP5 MMM (with both contributing about 5 Sv to the boundary current transport). We also note, like NOW (Figure 7h), there are only small changes in the Island Rule transport for Australia (Figure 8h), and the inferred MMM EAC change (12.4 Sv) is considerably larger than the projected change calculated from the velocity field (~6.5 Sv). This was also found by Sen Gupta et al. (2016).

4. Summary and Discussion

The NOW coupled regional climate model was introduced and evaluated in terms of the Tasman Sea circulation in observations (AVISO, RG94, CARS, and OISST) and previous modeling studies (BULL-2017 and BULL-2018). Compared to AVISO and BULL-2017/BULL-2018, the NOW historical (HIST) circulation shows a small improvement in sea surface height variability. It does, however, have an EACx bias where the EACx transport is substantially larger than observations. Ocean-only simulations over the same domain as NOW and with the same physics/boundary forcing (BULL-2017/BULL-2018) have more realistic transports (although still too high). As such, the difference between these simulations must relate to winds over the NOW domain. The linear response of the circulation to the winds, determined through an examination of the GIR estimated EAC transports, were unable to explain the large EACx HIST transport. The linear Island Rule theory omits the effects of bathymetry, advection, and the mean response to variable wind forcing. Investigation of the role of these would be an interesting avenue for future work.

The goal of this study was to use an eddy-permitting regional coupled climate model to better understand future CMIP5 projections. A hierarchy of NOW model simulations with historical and seasonal CMIP5 RCP8.5 climate change perturbations applied at the domain boundaries was examined to understand the impact of remote atmospheric and remote ocean forcing on projected changes in the Tasman Sea circulation (see section 2.2 for definition of "remote" forcing). Consistent with previous studies using coarse resolution climate models and eddy resolving ocean models, NOW (RCP85) projects a strongly enhanced EACx (12 Sv at JK in Figure 6 by the end of the century based on the CMIP5 RCP8.5 MMM forcing) and weaker Tasman

Front transport. A stronger EACx leads to 4.5°C warming in the southern Tasman Sea, 1°C warmer than the CMIP5 MMM. Additional experiments (RCP85-RAD, RCP85-OCE, and RCP85-ATM) show that the projected changes in the transport of the EACx are largely due (73% of mean EAC transport at JK) to future CMIP5 RCP85 anomalies applied on the atmospheric domain boundaries. The radiative forcing anomalies and anomalies at the ocean boundary (that would presumably be largely related to projected wind stress changes to the east of the NOW domain) play a much smaller role. We also use linear theory to infer the anticipated circulation changes resulting from changes to the wind field, and we find that the dominant role of the atmospheric boundary forcing on the projected EACx transport change is broadly consistent with the linear response to wind-stress changes over the western Pacific model domain. On the other hand, the CMIP5 MMM shows almost equal contributions from winds to the east and west of the NOW domain. In both the HIST evaluation (section 3.2) and the NOW projections (section 3.4), the NOW model simulates a transport that matches better with linear theory than the CMIP5 MMM.

Consistent with the Tasman Sea climate change literature, this study has shown that an enhanced EACx/weaker Tasman Front is likely under a business as usual scenario. We have additionally shown that *regional* changes in the atmospheric boundary condition are the main driver of this response, and that the changes in the NOW projection (RCP85) can be explained to first order by linear theory. This focus on regional changes is counter to work by O'Kane et al. (2014) and Sloyan and O'Kane (2015) suggesting that the EACx increase in strength in recent decades has been driven by basin-scale changes in wind stress curl. It does support work by Roemmich et al. (2007) which suggested that enhanced circulation of the subtropical gyre since the 1990s could be related to *regional* decadal changes in wind stress curl. Our focus on projected mean-state changes in surface winds for CMIP5 is supported by Lin et al. (2020) who showed that 10 out of 11 models with a significant increasing wind stress trend (1960–2005) are driven by increasing strength of the *mean* westerly wind. While we have only examined the effect of mean-state changes in surface winds, Bull et al. (2017) found a similar, *nonlinear* increase in EACx transport was possible (10.3 Sv, 99%, at JK) with the introduction of relatively high-frequency (<~2 months) regional atmospheric variability (with no change to time-mean wind stress). Lin et al. (2018) have shown that changes in wind variability intensity account for all or a large part (depending on reanalysis product) of the trend in mean westerly winds over the reanalysis period. Future work therefore could perturb a regional model with new projections of changes in wind stress variability as well as time-mean changes.

It remains unclear as to why the NOW-HIST simulation has a such a strong EACx compared to other similar ocean-only models BULL-2017 and BULL-2018 and to the observations. In particular, we note that while surface wind differences and linear theory can explain the projected changes, they were not able to explain the mean state differences. Other studies (e.g., Bull et al., 2018; Marchesiello & Middleton, 2000; Oke, Roughan, et al., 2019) have shown that the dynamics determining the mean EAC retroflection extent are highly nonlinear. Future work could utilize a NEMO ocean-only configuration with outputs from NOW to determine the source of this bias. Finally, this study does not address the likely importance of mesoscale atmosphere-ocean interactions (e.g., Ma et al., 2016; Renault et al., 2016; Renault, Molemaker, Gula, et al., 2016); work on characterizing these interactions (e.g., thermal and current feedbacks) and their influence on the mean circulation is ongoing. Some of those mesoscale interactions could explain local modifications in the wind stress curl compared to eddying ocean-only simulations, deprived of air-sea feedbacks, and coarser coupled models, deprived of mesoscale eddies.

Acknowledgments

For their roles in producing, coordinating, and making available CMIP5 model output (Table S1), we acknowledge the climate modeling groups, the World Climate Research Programme's Working Group on Coupled Modeling and the Global Organization for Earth System Science Portals. The altimeter products were produced and distributed by Aviso+ (https://www.aviso.altimetry.fr/), as part of the Ssalto ground processing segment. The AVISO product used is the daily, delayed time, all satellite, Mapped Absolute Dynamic Topography (DT-MADT) product consisting of the mean dynamic topography from MDT CNES-CLS13 (Rio et al., 2014) and Mapped Sea Level Anomalies from DUACS DT2014 (Pujol et al., 2016). This work was supported by the Australian Research Council (DP180101251) and the ARC Centre of Excellence in Climate System Science (CE110001028). Christopher Bull is supported through the Filchner Ice Shelf System (FISS) project NE/L013770/1. Daniel Argüeso is funded by the European Union's Horizon 2020 programme through a Marie Sklodowska-Curie Individual Fellowship (H2020-MSCA-IF-2016-743547). This research was undertaken with the assistance of resources from the National Computational Infrastructure (NCI), which is supported by the Australian Government. All model output generated in this study is archived in the UNSW Data Archive (https://dataarchive.unsw.edu.au). The scripts used to prepare the model configurations and the model components are available online (http://doi.org/10.5281/zenodo.3760905). The authors also acknowledge the comments of two anonymous reviewers which led to improvements in the manuscript.

References

Amante, C., & Eakins, B. W. (2009). ETOPO1 1 arc-minute global relief model: Procedures, data sources and analysis. *NOAA Technical Memorandum NESDIS NGDC-24*, (March), 19. https://doi.org/10.1594/PANGAEA.769615

Archer, M. R., Roughan, M., Keating, S. R., & Schaeffer, A. (2017). On the variability of the East Australian Current: Jet structure, meandering, and influence on shelf circulation. *Journal of Geophysical Research: Oceans*, *122*, 8464–8481. https://doi.org/10.1002/2017JC013097

Baird, M. E., & Ridgway, K. R. (2012). The southward transport of sub-mesoscale lenses of Bass Strait water in the centre of anti-cyclonic mesoscale eddies. *Geophysical Research Letters*, *39*, L05603. https://doi.org/10.1029/2011GL050643

Barnier, B., Dussin, R., & Molines, J. M. (2011). Scientific validation report (ScVR) for V1 reprocessed analysis and reanalysis. WP 04 – GLO – CNRS_LEGI Grenoble.

Biastoch, A., Böning, C. W., Schwarzkopf, F. U., & Lutjeharms, J. R. E. (2009). Increase in Agulhas leakage due to poleward shift of Southern Hemisphere westerlies. *Nature*, *462*(7272), 495–498. https://doi.org/10.1038/nature08519

Bowen, M. M., Wilkin, J. L., & Emery, W. J. (2005). Variability and forcing of the East Australian Current. *Journal of Geophysical Research*, *110*, C03019. https://doi.org/10.1029/2004JC002533

Bracegirdle, T. J., Shuckburgh, E., Sallee, J.-B., Wang, Z., Meijers, A. J. S., Bruneau, N., et al. (2013). Assessment of surface winds over the Atlantic, Indian, and Pacific Ocean sectors of the Southern Ocean in CMIP5 models: Historical bias, forcing response, and state dependence. *Journal of Geophysical Research: Atmospheres*, *118*, 547–562. https://doi.org/10.1002/jgrd.50153

Bull, C. Y. S., Kiss, A. E., Jourdain, N. C., England, M. H., & van Sebille, E. (2017). Wind forced variability in Eddy formation, Eddy shedding, and the separation of the East Australian Current. *Journal of Geophysical Research: Oceans*, *122*, 9980–9998. https://doi.org/10.1002/2017JC013311

Bull, C. Y. S., Kiss, A. E., van Sebille, E., Jourdain, N. C., & England, M. H. (2018). The role of the New Zealand Plateau in the Tasman Sea circulation and separation of the East Australian Current. *Journal of Geophysical Research: Oceans*, *123*, 1457–1470. https://doi.org/10.1002/2017JC013412

Cai, W. (2006). Antarctic ozone depletion causes an intensification of the Southern Ocean super-gyre circulation. *Geophysical Research Letters*, *33*, L03712. https://doi.org/10.1029/2005GL024911

Cai, W., Shi, G., Cowan, T., Bi, D., & Ribbe, J. (2005). The response of the southern annular mode, the East Australian Current, and the southern mid-latitude ocean circulation to global warming. *Geophysical Research Letters*, *32*, L23706. https://doi.org/10.1029/2005GL024701

Cai, W., Wang, G., Dewitte, B., Wu, L., Santoso, A., Takahashi, K., et al. (2018). Increased variability of eastern Pacific El Niño under greenhouse warming. *Nature*, *564*(7735), 201–206. https://doi.org/10.1038/s41586-018-0776-9

Chamberlain, M. A., Sun, C., Matear, R. J., Feng, M., & Phipps, S. J. (2012). Downscaling the climate change for oceans around Australia. *Geoscientific Model Development*, *5*(5), 1177–1194. https://doi.org/10.5194/gmd-5-1177-2012

Dee, D. P., Uppala, S. M., Simmons, A. J., Berrisford, P., Poli, P., Kobayashi, S., et al. (2011). The ERA-interim reanalysis: Configuration and performance of the data assimilation system. *Quarterly Journal of the Royal Meteorological Society*, *137*(656), 553–597. https://doi.org/10.1002/qj.828

Di Luca, A., Evans, J. P., Pepler, A. S., Alexander, L. V., & Argüeso, D. (2016). Evaluating the representation of Australian East Coast Lows in a regional climate model ensemble. *Journal of Southern Hemisphere Earth Systems Science*, *66*(2), 108–124. https://doi.org/10.22499/3.6002.003

Di Virgilio, G., Evans, J. P., Di Luca, A., Olson, R., Argüeso, D., Kala, J., et al. (2019). Evaluating reanalysis-driven CORDEX regional climate models over Australia: Model performance and errors. *Climate Dynamics*, *53*(5–6), 2985–3005. https://doi.org/10.1007/s00382-019-04672-w

Durgadoo, J. V., Loveday, B. R., Reason, C. J. C., Penven, P., & Biastoch, A. (2013). Agulhas leakage predominantly responds to the Southern Hemisphere Westerlies. *Journal of Physical Oceanography*, *43*(10), 2113–2131. https://doi.org/10.1175/JPO-D-13-047.1

Dussin, R., Molines, J., & Barnier, B. (2012). Definition of the interannual experiment ORCA025.L75-GRD100, 1958-2010.

Elipot, S., & Beal, L. M. (2018). Observed Agulhas Current sensitivity to interannual and long-term trend atmospheric forcings. *Journal of Climate*, JCLI-D-17-0597.1. https://doi.org/10.1175/JCLI-D-17-0597.1

Everett, J. D., Baird, M. E., Oke, P. R., & Suthers, I. M. (2012). An avenue of eddies: Quantifying the biophysical properties of mesoscale eddies in the Tasman Sea. *Geophysical Research Letters*, *39*, L16608. https://doi.org/10.1029/2012GL053091

Feng, M., Zhang, X., Oke, P., Monselesan, D., Chamberlain, M., Matear, R., & Schiller, A. (2016). Invigorating ocean boundary current systems around Australia during 1979–2014: As simulated in a near-global eddy-resolving ocean model. *Journal of Geophysical Research: Oceans*, *121*, 3395–3408. https://doi.org/10.1002/2015JC011486.Received

Fernandez, D., Bowen, M., & Sutton, P. (2018). Variability, coherence and forcing mechanisms in the New Zealand ocean boundary currents. *Progress in Oceanography*, *165*(April), 168–188. https://doi.org/10.1016/j.pocean.2018.06.002

Godfrey, J. S. (1989). A Sverdrup model of the depth-integrated flow for the world ocean allowing for island circulations. *Geophysical and Astrophysical Fluid Dynamics*, *45*(1–2), 89–1-2. https://doi.org/10.1080/03091928908208894, 112

Godfrey, J. S., & Dunn, J. R. (2010). Depth-integrated steric height as a tool for detecting non-Sverdrup behavior in the global ocean. *Journal of Marine Research*, *68*(3), 387–412. https://doi.org/10.1357/002224010794657100

Gray, A. R., & Riser, S. C. (2014). A global analysis of Sverdrup balance using absolute geostrophic velocities from Argo. *Journal of Physical Oceanography*, *44*(4), 1213–1229. https://doi.org/10.1175/JPO-D-12-0206.1

Haarsma, R. J., Roberts, M., Vidale, P. L., Senior, C. A., Bellucci, A., Bao, Q., et al. (2016). High Resolution Model Intercomparison Project (HighResMIP). *Geoscientific Model Development Discussion*, (April), 1–35. https://doi.org/10.5194/gmd-2016-66

Hallberg, R. (2013). Using a resolution function to regulate parameterizations of oceanic mesoscale eddy effects. *Ocean Modelling*, *72*, 92–103. https://doi.org/10.1016/j.ocemod.2013.08.007

Hill, K. L., Rintoul, S. R., Ridgway, K. R., & Oke, P. R. (2011). Decadal changes in the South Pacific western boundary current system revealed in observations and ocean state estimates. *Journal of Geophysical Research*, *116*, C01009. https://doi.org/10.1029/2009JC005926

Hu, D., Wu, L., Cai, W., Gupta, A. S., Ganachaud, A., Qiu, B., et al. (2015). Pacific western boundary currents and their roles in climate. *Nature*, *522*(7556), 299–308. https://doi.org/10.1038/nature14504

Janjić, Z. I. (1994). The step-mountain eta coordinate model: Further developments of the convection, viscous sublayer, and turbulence closure schemes. *Monthly Weather Review*, *122*(5), 927–945. https://doi.org/10.1175/1520-0493(1994)122%3C0927:TSMECM%3E2.0.CO;2

Kiss, A. E., Hogg, A. M., Hannah, N., Boeira Dias, F., Brassington, G. B., Chamberlain, M. A., et al. (2020). ACCESS-OM2 v1.0: A global ocean–sea ice model at three resolutions. *Geoscientific Model Development*, 1–58. https://doi.org/10.5194/gmd-2019-106

Knutson, T. R., Sirutis, J. J., Garner, S. T., Vecchi, G. A., & Held, I. M. (2008). Simulated reduction in Atlantic hurricane frequency under twenty-first-century warming conditions. *Nature Geoscience*, *1*(6), 359–364. https://doi.org/10.1038/ngeo202

Krinner, G., & Flanner, M. G. (2018). Striking stationarity of large-scale climate model bias patterns under strong climate change. *Proceedings of the National Academy of Sciences*, *115*(38), 9462–9466. https://doi.org/10.1073/pnas.1807912115

Li, Y., Jourdain, N. C., Taschetto, A. S., Gupta, A. S., Argüeso, D., Masson, S., & Cai, W. (2016). Resolution dependence of the simulated precipitation and diurnal cycle over the Maritime Continent. *Climate Dynamics*, *48*(11-12), 4009–4028. https://doi.org/10.1007/s00382-016-3317-y

Lin, X., Zhai, X., Wang, Z., & Munday, D. R. (2018). Mean, variability, and trend of Southern Ocean wind stress: Role of wind fluctuations. *Journal of Climate*, *31*(9), 3557–3573. https://doi.org/10.1175/JCLI-D-17-0481.1

Lin, X., Zhai, X., Wang, Z., & Munday, D. R. (2020). Southern Ocean wind stress in CMIP5 models: Role of wind fluctuations. *Journal of Climate*, *33*(4), 1209–1226. https://doi.org/10.1175/jcli-d-19-0466.1

Loveday, B. R., Durgadoo, J. V., Reason, C. J. C., Biastoch, A., & Penven, P. (2014). Decoupling of the Agulhas leakage from the Agulhas Current. *Journal of Physical Oceanography*, *44*(7), 1776–1797. https://doi.org/10.1175/JPO-D-13-093.1

Ma, X., Jing, Z., Chang, P., Liu, X., Montuoro, R., Small, R. J., et al. (2016). Western boundary currents regulated by interaction between ocean eddies and the atmosphere. *Nature*, *535*(7613), 533–537. https://doi.org/10.1038/nature18640

Madec, G. (2012). NEMO ocean engine. *Note Du Pôle de Modélisation, Institut Pierre-Simon Laplace (IPSL)* (Vol. 27, p. 357). Retrieved from. http://eprints.soton.ac.uk/64324/

Marchesiello, P., & Middleton, J. H. (2000). Modeling the East Australian Current in the Western Tasman Sea. *Journal of Physical Oceanography*, *30*(11), 2956–2971. https://doi.org/10.1175/1520-0485(2001)031%3C2956:MTEACI%3E2.0.CO;2

Mata, M. M., Wijffels, S. E., Church, J. A., & Tomczak, M. (2006). Eddy shedding and energy conversions in the East Australian Current. *Journal of Geophysical Research*, *111*, C09034. https://doi.org/10.1029/2006JC003592

Matear, R. J., Chamberlain, M. A., Sun, C., & Feng, M. (2013). Climate change projection of the Tasman Sea from an Eddy-resolving Ocean Model. *Journal of Geophysical Research: Oceans*, *118*, 2961–2976. https://doi.org/10.1002/jgrc.20202

Matear, R. J., Chamberlain, M. A., Sun, C., & Feng, M. (2015). Climate change projection for the western tropical Pacific Ocean using a high-resolution ocean model: Implications for tuna fisheries. *Deep-Sea Research Part II: Topical Studies in Oceanography*, *113*(July), 22–46. https://doi.org/10.1016/j.dsr2.2014.07.003

O'Kane, T. J., Matear, R. J., Chamberlain, M. A., Oliver, E. C. J., & Holbrook, N. J. (2014). Storm tracks in the Southern Hemisphere subtropical oceans. *Journal of Geophysical Research: Oceans*, *119*, 6078–6100. https://doi.org/10.1002/2014JC010192.Received

Oerder, V., Colas, F., Echevin, V., Masson, S., Hourdin, C., Jullien, S., et al. (2016). Mesoscale SST–wind stress coupling in the Peru-Chile current system: Which mechanisms drive its seasonal variability? *Climate Dynamics*, *47*(7–8), 2309–2330. https://doi.org/10.1007/s00382-015-2965-7

Oke, P. R., Pilo, G. S., Ridgway, K., Kiss, A., & Rykova, T. (2019). A search for the Tasman Front. *Journal of Marine Systems*, *199*(May), 103217. https://doi.org/10.1016/j.jmarsys.2019.103217

Oke, P. R., Roughan, M., Cetina-Heredia, P., Pilo, G. S., Ridgway, K. R., Rykova, T., et al. (2019). Revisiting the circulation of the East Australian Current: Its path, separation, and eddy field. *Progress in Oceanography*, *176*(November 2018), 102139. https://doi.org/10.1016/j.pocean.2019.102139

Oliver, E. C. J., & Holbrook, N. J. (2014). Extending our understanding of South Pacific gyre 'spin-up': Modelling the East Australian Current in a future climate. *Journal of Geophysical Research: Oceans*, *119*, 2788–2805. https://doi.org/10.1002/2013JC009591

Oliver, E. C. J., O'Kane, T. J., Holbrook, N. J., Kane, T. J. O., & Holbrook, N. J. (2015). Projected changes to Tasman Sea eddies in a future climate. *Journal of Geophysical Research: Oceans*, *120*, 2331–2349.

Oliver, E. C. J., Wotherspoon, S. J., Chamberlain, M. a., & Holbrook, N. J. (2013). Projected Tasman Sea extremes in sea surface temperature through the twenty-first century. *Journal of Climate*, *27*(5), 1980–1998. https://doi.org/10.1175/JCLI-D-13-00259.1

Pilo, G. S., Oke, P. R., Rykova, T., Coleman, R., & Ridgway, K. (2015). Do East Australian Current anticyclonic eddies leave the Tasman Sea? *Journal of Geophysical Research: Oceans*, *120*, 8099–8114. https://doi.org/10.1002/2015JC011026

Pujol, M. I., Faugère, Y., Taburet, G., Dupuy, S., Pelloquin, C., Ablain, M., & Picot, N. (2016). DUACS DT2014: The new multi-mission altimeter data set reprocessed over 20 years. *Ocean Science*, *12*(5), 1067–1090. https://doi.org/10.5194/os-12-1067-2016

Renault, L., McWilliams, J. C., & Penven, P. (2017). Modulation of the Agulhas Current retroflection and leakage by oceanic current interaction with the atmosphere in coupled simulations. *Journal of Physical Oceanography*, *47*(8), 2077–2100. https://doi.org/10.1175/JPO-D-16-0168.1

Renault, L., Molemaker, M. J., Gula, J., Masson, S., & McWilliams, J. C. (2016). Control and stabilization of the Gulf Stream by oceanic current interaction with the atmosphere. *Journal of Physical Oceanography*, JPO-D-16-0115.1. https://doi.org/10.1175/JPO-D-16-0115.1

Renault, L., Molemaker, M. J., McWilliams, J. C., Shchepetkin, A. F., Lemarié, F., Chelton, D., et al. (2016). Modulation of wind-work by oceanic current interaction with the atmosphere. *Journal of Climate*, *46*(6), 1685–1704. https://doi.org/10.1175/JPO-D-15-0232.1

Ridgway, K., Dunn, J. R., & Wilkin, J. L. (2002). Ocean interpolation by four-dimensional weighted least squares—Application to the waters around Australasia. *Journal of Atmospheric and Oceanic Technology*, *19*(9), 1357–1375. https://doi.org/10.1175/1520-0426(2002)019%3C1357:OIBFDW%3E2.0.CO;2

Ridgway, K. R. (2007). Long-term trend and decadal variability of the southward penetration of the East Australian Current. *Geophysical Research Letters*, *34*, L13613. https://doi.org/10.1029/2007GL030393

Ridgway, K. R., Coleman, R. C., Bailey, R. J., & Sutton, P. (2008). Decadal variability of East Australian Current transport inferred from repeated high-density XBT transects, a CTD survey and satellite altimetry. *Journal of Geophysical Research*, *113*, C08039. https://doi.org/10.1029/2007JC004664

Ridgway, K. R., & Dunn, J. (2003). Mesoscale structure of the mean East Australian Current System and its relationship with topography. *Progress in Oceanography*, *56*(2), 189–222. https://doi.org/10.1016/S0079-6611(03)00004-1

Ridgway, K. R., & Godfrey, J. S. (1994). Mass and heat budgets in the East Australian Current: A direct approach. *Journal of Geophysical Research*, *99*(C2), 3231–3248. https://doi.org/10.1029/93JC02255

Ridgway, K. R., & Godfrey, J. S. (1997). Seasonal cycle of the East Australian Current. *Journal of Geophysical Research*, *102*(C10), 22,921–22,936. https://doi.org/10.1029/97JC00227

Rio, M. H., Mulet, S., & Picot, N. (2014). Beyond GOCE for the ocean circulation estimate: Synergetic use of altimetry, gravimetry, and in situ data provides new insight into geostrophic and Ekman currents. *Geophysical Research Letters*, *41*, 8918–8925. https://doi.org/10.1002/2014GL061773

Roemmich, D., Gilson, J., Davis, R., Sutton, P., Wijffels, S., & Riser, S. (2007). Decadal spinup of the South Pacific subtropical gyre. *Journal of Physical Oceanography*, *37*(2), 162–173. https://doi.org/10.1175/JPO3004.1

Roemmich, D., Gilson, J., Sutton, P., & Zilberman, N. (2016). Multidecadal change of the South Pacific gyre circulation. *Journal of Physical Oceanography*, *46*(6), 1871–1883. https://doi.org/10.1175/JPO-D-15-0237.1

Samson, G., Masson, S., Lengaigne, M., Keerthi, M. G., Vialard, J., Pous, S., et al. (2014). The NOW regional coupled model: Application to the tropical Indian Ocean climate and tropical cyclone activity. *Journal of Advances in Modeling Earth Systems*, *6*, 223–248. https://doi.org/10.1002/2014MS000324

Sato, T., Kimura, F., & Kitoh, A. (2007). Projection of global warming onto regional precipitation over Mongolia using a regional climate model. *Journal of Hydrology*, *333*(1), 144–154. https://doi.org/10.1016/j.jhydrol.2006.07.023

Sen Gupta, A., McGregor, S., van Sebille, E., Ganachaud, A., Brown, J., & Santoso, A. (2016). Future changes to the Indonesian Throughflow and Pacific circulation: The role of wind and deep circulation changes. *Geophysical Research Letters*, *43*, 1669–1678. https://doi.org/10.1002/2016GL067757

Skamarock, W. C., Klemp, J. B., Dudhi, J., Gill, D. O., Barker, D. M., Duda, M. G., et al. (2008). A description of the advanced research WRF version 3. *Technical Report*, (June), 113. https://doi.org/10.5065/D6DZ069T

Sloyan, B. M., & O'Kane, T. J. (2015). Oceans drivers of decadal variability in the Tasman Sea. *Journal of Geophysical Research: Oceans*, *120*, 3193–3210. https://doi.org/10.1002/2014JC010550

Sloyan, B. M., Ridgway, K. R., & Cowley, R. (2016). The East Australian Current and property transport at 27 S from 2012-2013. *Journal of Physical Oceanography*, *46*(3), 993–1008. https://doi.org/10.1175/JPO-D-15-0052.1

Speich, S., Blanke, B., De Vries, P., Drijfhouté, S., Döös, K., & Ganachaud, A. (2002). Tasman leakage: A new route in the global ocean conveyor belt. *Geophysical Research Letters*, *29*(10), 55-1–55-4. https://doi.org/10.1029/2001GL014586

Sun, C., Feng, M., Matear, R. J., Chamberlain, M. a., Craig, P., Ridgway, K. R., & Schiller, A. (2012). Marine downscaling of a future climate scenario for Australian boundary currents. *Journal of Climate*, *25*(8), 2947–2962. https://doi.org/10.1175/JCLI-D-11-00159.1

Sverdrup, H. U. (1947). Wind-driven currents in a Baroclinic Ocean; with application to the equatorial currents of the eastern Pacific. *Proceedings of the National Academy of Sciences*, *33*(11), 318–326. https://doi.org/10.1073/pnas.33.11.318

Swart, N. C., & Fyfe, J. C. (2012). Observed and simulated changes in the Southern Hemisphere surface westerly wind-stress. *Geophysical Research Letters*, *39*, L16711. https://doi.org/10.1029/2012GL052810

Szoeke, R. A. De (1987). On the wind-driven circulation of the South Pacific Ocean. *Journal of Physical Oceanography*, *17*, 613–630. https://doi.org/10.1175/1520-0485

Tilburg, C. E., Hurlburt, H. E., O'Brien, J. J., & Shriver, J. F. (2001). The dynamics of the East Australian Current system: The Tasman Front, the East Auckland Current, and the east cape current. *Journal of Physical Oceanography*, *31*(10), 2917–2943. https://doi.org/10.1175/1520-0485(2001)031%3C2917:TDOTEA%3E2.0.CO;2

Valcke, S. (2013). The OASIS3 coupler: A European climate modelling community software. *Geoscientific Model Development*, *6*(2), 373–388. https://doi.org/10.5194/gmd-6-373-2013

Wajsowicz, R. C. (1993). The circulation of the depth-integrated flow around an island with application to the Indonesian Throughflow. *Journal of Physical Oceanography*, *23*(7), 1470–1484. https://doi.org/10.1175/1520-0485(1993)023%3C1470:TCOTDI%3E2.0.CO;2

Walsh, K. (2015). Fine resolution simulations of the effect of climate change on tropical cyclones in the South Pacific. *Climate Dynamics*, *45*(9–10), 2619–2631. https://doi.org/10.1007/s00382-015-2497-1

Wang, G., Cai, W., & Purich, A. (2014). Trends in Southern Hemisphere wind-driven circulation in CMIP5 models over the 21st century: Ozone recovery versus greenhouse forcing. *Journal of Geophysical Research: Oceans*, *119*, 2974–2986. https://doi.org/10.1002/2013JC009589

Wang, X. H., Bhatt, V., & Sun, Y.-J. (2013). Study of seasonal variability and heat budget of the East Australian Current using two eddy-resolving ocean circulation models. *Ocean Dynamics*, *63*(5), 549–563. https://doi.org/10.1007/s10236-013-0605-5

Wu, L., Cai, W., Zhang, L., Nakamura, H., Timmermann, A., Joyce, T., et al. (2012). Enhanced warming over the global subtropical western boundary currents. *Nature Climate Change*, *2*(3), 161–166. https://doi.org/10.1038/nclimate1353

Yang, H., Lohmann, G., Wei, W., Dima, M., Ionita, M., & Liu, J. (2016). Intensification and poleward shift of subtropical western boundary currents in a warming climate. *Journal of Geophysical Research: Oceans*, *121*, 4928–4945. https://doi.org/10.1002/2015JC011421. Received

Yoshikane, T., Kimura, F., Kawase, H., & Nozawa, T. (2012). Verification of the performance of the pseudo-global-warming method for future climate changes during June in East Asia. *Scientific Online Letters on the Atmosphere*, *8*(0), 133–136. https://doi.org/10.2151/sola.2012-033

Ypma, S. L., van Sebille, E., Kiss, A. E., & Spence, P. (2016). The separation of the East Australian Current: A Lagrangian approach to potential vorticity and upstream control. *Journal of Geophysical Research: Oceans*, *120*, 2331–2349. https://doi.org/10.1002/2014JC010632